

A Framework for the Analysis of Computational Imaging Systems with Practical Applications

Kaushik Mitra, *Member, IEEE*, Oliver S. Cossairt, *Member, IEEE*
and Ashok Veeraraghavan, *Member, IEEE*

arXiv:1308.1981v1 [cs.CV] 8 Aug 2013

Abstract—Over the last decade, a number of Computational Imaging (CI) systems have been proposed for tasks such as motion deblurring, defocus deblurring and multispectral imaging. These techniques increase the amount of light reaching the sensor via multiplexing and then undo the deleterious effects of multiplexing by appropriate reconstruction algorithms. Given the widespread appeal and the considerable enthusiasm generated by these techniques, a detailed performance analysis of the benefits conferred by this approach is important.

Unfortunately, a detailed analysis of CI has proven to be a challenging problem because performance depends equally on three components: (1) the optical multiplexing, (2) the noise characteristics of the sensor, and (3) the reconstruction algorithm which typically uses signal priors. A few recent papers [10], [9], [42] have performed analysis taking multiplexing and noise characteristics into account. However, analysis of CI systems under state-of-the-art reconstruction algorithms, most of which exploit signal prior models, has proven to be unwieldy. In this paper, we present a comprehensive analysis framework incorporating all three components.

In order to perform this analysis, we model the signal priors using a Gaussian Mixture Model (GMM). A GMM prior confers two unique characteristics. Firstly, GMM satisfies the universal approximation property which says that any prior density function can be approximated to any fidelity using a GMM with appropriate number of mixtures. Secondly, a GMM prior lends itself to analytical tractability allowing us to derive simple expressions for the ‘minimum mean square error’ (MMSE) which we use as a metric to characterize the performance of CI systems. We use our framework to analyze several previously proposed CI techniques (focal sweep, flutter shutter, parabolic exposure, etc.), giving conclusive answer to the question: ‘How much performance gain is due to use of a signal prior and how much is due to multiplexing? Our analysis also clearly shows that multiplexing provides significant performance gains above and beyond the gains obtained due to use of signal priors.

Index Terms—Computational imaging, Extended depth-of-field (EDOF), Motion deblurring, GMM

1 INTRODUCTION

Computational Imaging systems can be broadly categorized into two categories [37]: those designed either to add a new functionality or to increase performance relative to a conventional imaging system. A light field camera [38], [47], [27], [34] is an example of the former: it can be used to refocus or change perspective *after* images are captured - a functionality impossible to achieve with a conventional camera. The latter type of systems are the focus of this

- K. Mitra and A. Veeraraghavan are with the Department of Electrical and Computer Engineering, Rice University, Houston, TX, 77025. E-mail: Kaushik.Mitra@rice.edu and vashok@rice.edu
- O. S. Cossairt is with the Department of Electrical Engineering and Computer Science, Northwestern University, Evanston, IL 60208. E-mail: ollie@eecs.northwestern.edu

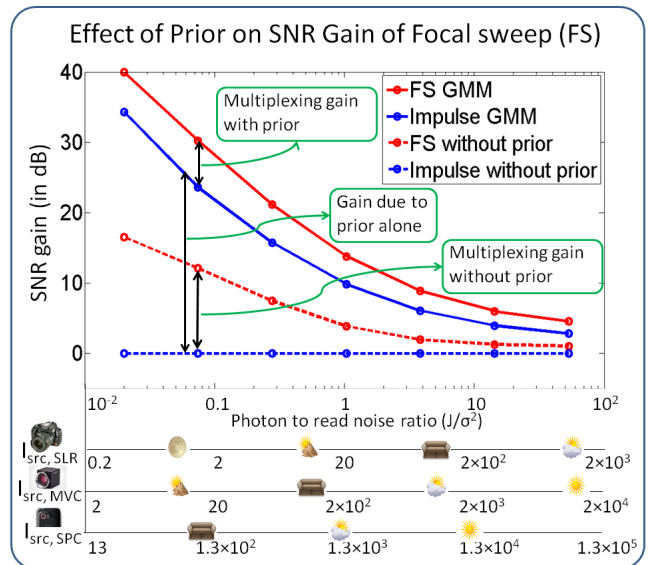


Fig. 1. *Effect of signal prior on multiplexing gain of focal sweep [26]:* We show the multiplexing gain of focal sweep over impulse imaging (a conventional camera with stopped down aperture) at different photon to read noise ratios J/σ_r^2 . The photon to read noise ratio is related to illumination level and camera specifications. In the extended x-axis, corresponding to different values of J/σ_r^2 , we show the light levels (in lux) for three camera types: a high end SLR, a machine vision camera (MVC) and a smartphone camera (SPC). As shown by Cossairt et al. [10], without using signal priors, we get a huge multiplexing gain at low J/σ_r^2 . But with a signal prior (GMM) the multiplexing gain is modest even at low J/σ_r^2 . Thus, this figure clearly shows the importance of analyzing CI systems with signal priors taken into account.

paper, and from here on we use the term CI to refer to them. Examples include extended depth-of-field (EDOF) systems [28], [47], [53], [24], [26], [13], [23], [30], [18], [5], [39], [17], motion deblurring [41], [33], [8], spectroscopy [21], [20], [48], color imaging [4], [25], multiplexed light field acquisition [47], [27], [34] and illumination multiplexing [44], [42]. These systems use optical coding (multiplexing) to increase light throughput, which increases the SNR of

captured images. The desired signal is then recovered computationally via signal processing. The quality of recovered images depends jointly on the conditioning of the optical coding and the increased light throughput. A poor choice of multiplexing will reduce image quality.

The question of exactly how much performance improvement can be achieved via multiplexing has received a fair amount of attention in the literature [21], [9], [10], [25], [44], [49], [42], [23], [22]. It is well understood that multiplexing gives the greatest advantage at low light levels (where *signal-independent* read noise dominates), but this advantage diminishes with increasing light (where *signal-dependent* photon noise dominates) [21]. However, it is impractical to study the effects of multiplexing alone, since signal priors are at the heart of every state-of-the-art reconstruction algorithm (e.g. dictionary learning [2], BM3D [12], GMM [51], [36]). Signal priors can dramatically increase performance in problems of deblurring (multiplexed sensing) and denoising (no multiplexing), typically with greater improvement as noise increases (i.e. as the light level decreases). While both signal priors and multiplexing increase performance at low light levels, the former is trivial to incorporate and the latter often requires hardware modifications. Thus, it is imperative to understand the improvement due to multiplexing *above and beyond* that due to signal priors. However, comprehensive analysis of CI systems remains an elusive problem because state-of-the-art priors often use signal models unfavorable to analysis.

In this work, we follow a line of research whose goal is to derive bounds on the performance of CI systems [42], [25], and relate maximum performance to practical considerations (e.g. illumination conditions and sensor characteristics) [10]. We follow the convention adopted by Cossairt et al. [10]. We define a conventional camera as an *impulse imaging system* which measures the desired signal directly (e.g. without blur). CI performance is then compared against the impulse imaging system. Noise is related to the lighting level, scene properties and sensor characteristics. In this paper, we pay special attention to the problems of defocus and motion blur. This type of blur can be position dependent when objects in the scene span either a range of depths or velocities. Various techniques have been devised to encode blur so as to make it either well-conditioned or position-independent (shift-invariant), or both. For defocus deblurring, CI systems encode defocus blur using attenuation masks [28], [47], [53], refractive masks [13], or motion [24], [26]. The impulse imaging counterpart is a narrow aperture image with no defocus blur. For motion deblurring, CI systems encode motion blur using a fluttered shutter [41] or camera motion [33], [8]. The impulse imaging counterpart is an image with short exposure time and no motion blur. Cossairt et al. derived an upper bound stating that the maximum gain due to multiplexing is quite large at low light levels. For example, in Figure 1, the multiplexing gain of focal sweep is > 10 dB for a low photon to read noise ratio < 0.1 . However, as we show in this paper, this makes for an exceptionally weak bound because signal priors are not taken into account

In practice, signal priors can be used to improve the performance of any camera, impulse and computational alike. Since incorporating a signal prior can be done merely by applying an algorithm to captured images, it is natural to expect that we would always choose to do so. However, it has historically been very difficult to determine exactly how much of an increase in performance to expect from signal priors, making it difficult to provide a fair comparison between different cameras.

We present a comprehensive framework that allows us to analyze the performance of CI systems while simultaneously taking into account multiplexing, sensor noise, and signal priors. We characterize the performance of CI systems under a GMM prior which has two unique properties: Firstly, GMM satisfies the universal approximation property which says that any probability density function (with a finite number of discontinuities) can be approximated to any fidelity using a GMM with an appropriate number of mixtures [45], [40]. Secondly, a GMM prior lends itself to analytical tractability allowing us to derive simple expressions for the MMSE, which we use as a metric to characterize the performance of both impulse and computational imaging systems. We use our framework to analyze several previously proposed CI techniques (focal sweep, flutter shutter, parabolic exposure, etc.), giving conclusive answers to the questions: ‘How much gain is due to the use of a signal prior and how much is due to multiplexing? What is the multiplexing gain above and beyond that due to use of a signal prior?’.

We show that the SNR benefits due to the use of a signal prior alone are quite large in low light and decrease as the light level increases (see Figure 1). We then provide comparisons between different cameras when signal priors are taken into account. We show that multiplexing provides a performance gain above and beyond the gain offered by the use of signal priors (as much as 6 – 9 dB in Figure 4). This indicates that CI techniques uniformly improve the performance of traditional imaging over a wide range of light levels above and beyond the benefits conferred due to sophisticated reconstruction algorithms.

1.1 Key Contributions

- 1) We extend the analysis of CI systems to include signal priors. Our analysis is based on the GMM prior, which can approximate almost any probability density function and is analytically tractable.
- 2) We use the GMM prior to quantify exactly how much the use of signal priors can improve the performance of a given camera. We derive an expression for the maximum performance of any camera that depends only on the parameters for the camera, noise, and learned signal prior.
- 3) We derive bounds on the performance of CI systems *with signal priors taken into account*. We show that the maximum increase in SNR *due to multiplexing alone* can be significant (about 9 dB for defocus deblurring cameras, see Figure 4, and 7 dB for motion deblurring, see Figure 5). This performance gain is much more modest than predicted previously [10],

but conclusively establishes the advantage of using multiplexing above and beyond the use of image priors.

1.2 Scope and Limitations

Image Formation Model. Our analysis assumes a linear image formation model. Non-linear imaging systems, such as a two/three photon microscopes and coherent imaging systems are outside the scope of this paper. Nevertheless, our analysis covers a very large array of existing imaging systems [41], [47], [28], [48], [25], [42]. We use a geometric optics model and ignore the effect of diffraction due to small apertures.

Noise Model. We use an affine noise model to describe the combined effects of *signal-independent* and *signal-dependent* noise. Signal-dependent Poisson noise is approximated using a Gaussian noise model (as described in Section 3.2).

Single Image Capture. We perform analysis of only single image CI techniques. Our results are therefore not applicable to multi-image capture techniques such as Hasinoff et al. [22] (EDOF), and Zhang et al. [52] (Motion Deblurring).

Patch Based Prior. Learning a GMM prior on entire images would require an impossibly large training set. To combat this problem, we train our GMM on image patches, and solve the image estimation problem in a patch-wise manner. As a result, our technique requires that multiplexed measurements are restricted to linear combinations of pixels in a neighborhood smaller than the GMM patch size.

Shift-Invariant Blur. We analyze motion and defocus deblurring cameras under the assumption of a single known shift-invariant blur kernel. This amounts to the assumption that either the depth/motion is position-independent, or the blur is independent of depth/motion. We do not analyze errors due to inaccurate kernel estimation (for coded aperture and flutter shutter [41], [47], [28]) or due to the degree of depth/motion invariance (for focal sweep, cubic phase plate, motion invariant photography [11], [3], [33], [8]).

2 RELATED WORK

Theoretical Analysis of CI systems: Harwit and Sloan [21] analyzed coded imaging systems and have shown that, in absence of photon noise, Hadamard and S-matrices are optimal. Wuttig and Ratner et al. [49], [42], [43] then extended the analysis to include both photon and read noise and showed that there is significant gain in multiplexing only when the read noise dominates over photon noise. Ihrke et. al. [25] analyzed the performance of different light field cameras and color filter arrays. Tendero [46] has analyzed the performance of flutter shutter cameras with respect of impulse imaging (short exposure imaging). Agarwal and Raskar compared the performance of flutter shutter and motion invariant cameras [1]. Recently, Cossairt et. al. [10], [9] has obtained optics independent upper bounds on performance for various CI techniques. They have shown that CI techniques have significant performance advantage over impulse imaging only when the average

signal level is below the read noise variance. However, all the above works, do not analyze the performance of CI systems when a signal prior is used for demultiplexing. Cossairt et al. [10] have performed empirical experiments to study the effect of priors, but conclusions drawn based from simulations are usually limited.

Performance Analysis using Image Priors: In the context of defocus deblurring, Zhou et al. [53] have used a Gaussian signal prior and Gaussian noise model to search for good aperture codes. In the context of light field imaging (LF), Levin et al. [29] have proposed the use of a GMM light field prior for comparing across different LF camera designs. They have used the mean square error as a metric for comparing the cameras. However, they do not take into account the effect of lighting level and photon noise.

Our approach is inspired in part by the recent analysis on the fundamental limits of the performance of image denoising [6], [31], [32], the only papers that we are aware of that directly address the issue of performance bounds in the presence of image priors. Both of these recent results, model image statistics through a patch based image prior and derive lower bounds on the MMSE for the problem of image denoising. We loosely follow the approach here and extend the analysis to general computational imaging systems. In order to render both computational tractability and generality, we use a GMM with a sufficient number of mixtures to model the prior distribution on image patches. Similar to [6], [31], [32], we then derive bounds and estimates for the MMSE and use these to analyze CI systems.

Practical Implications for CI systems: Cossairt et. al. [10] have analyzed CI systems taking into consideration the application (e.g. defocus deblurring or motion deblurring), lighting condition (e.g. moonlit night or sunny day), scene properties (e.g. albedo, object velocity) and sensor characteristics (size of pixels). They have shown that, for commercial grade image sensors, CI techniques can only provide a significant advantage over impulse imaging when the illumination is less than 125 lux (typical living room lighting). We extend these results to include the analysis of CI systems with signal priors taken into account. Hasinoff et al. [22] (in the context of EDOF) and Zhang et al. [52] (in the context of motion deblurring) have analyzed the trade-off between denoising and deblurring for multi-shot imaging within a time budget. We analyzed the trade-off between denoising and deblurring for single shot capture.

3 PROBLEM DEFINITION AND NOTATION

We consider linear multiplexed imaging systems that can be represented as

$$y = Hx + n, \quad (1)$$

where $y \in R^N$ is the measurement vector, $x \in R^N$ is the unknown signal we want to capture, H is the $N \times N$ multiplexing matrix and n is the observation noise.

3.1 Multiplexing Matrix H

A large array of existing imaging systems follow a linear image formation model, such as flutter shutter [41], coded

aperture [47], [28], [48], plenoptic multiplexing [25], illumination multiplexing [44], and many others. The results of this paper can be used to analyze all such systems. In this paper, we pay close attention to motion and defocus deblurring systems which produce shift-invariant blur. For the case of 1D motion blur, the vectors x and y represent a scanline in a sharp and blurred image patch, respectively. The multiplexing matrix H is a Toeplitz matrix where the rows contain the system point spread function. For the case of 2D defocus blur, the vectors x and y represent lexicographically reordered image patches, and the multiplexing matrix H is block Toeplitz.

3.2 Noise Model

To enable tractable analysis, we use an affine noise model [44], [22]. We model signal independent noise as a Gaussian random variable with variance σ_r^2 . Signal dependent photon noise is Poisson distributed with parameter λ equal to the average signal intensity at a pixel. We approximate photon noise by a Gaussian distribution with mean and variance λ . This is a good approximation when λ is greater than 10. We also drop the pixel-wise dependence of photon noise and instead assume that the noise variance at every pixel is equal to the average signal intensity.

3.3 Signal Prior Model

In this paper, we choose to model scene priors using a GMM because of three characteristics:

- **State of the art performance:** GMM priors have provided state of the art results in various imaging applications such as image denoising, deblurring and superresolution [51], [19], still-image CS [51], [7], light field denoising and superresolution [36] and video compressive sensing [50]. GMM is also closely related to the union-of-subspace model [15], [14] as each Gaussian mixture covariance matrix defines a principle subspace. GMM reconstruction can be interpreted as the weighted linear combination of subspace projections, which is closely related to dictionary learning and compressive sensing based reconstruction algorithms. Therefore, performance analysis of GMM models will track several nonlinear reconstruction algorithm performances faithfully.
- **Universal Approximation Property:** GMM satisfies the universal approximation property i.e., (almost) any prior can be approximated by learning a GMM with a large enough number of mixtures [45], [40]. To state this concisely, consider a family of zero mean Gaussian distributions $\mathcal{N}_\lambda(x)$ with variance λ . Let $p(x)$ be a prior probability density function with a finite number of discontinuities, that we want to approximate using a GMM distribution. Then the following Lemma holds:

Lemma 3.1: The sequence $p_\lambda(x)$ which is formed by the convolution of $\mathcal{N}_\lambda(x)$ and $p(x)$

$$p_\lambda(x) = \int_{-\infty}^{\infty} \mathcal{N}_\lambda(x-u)p(u)d(u) \quad (2)$$

converges uniformly to $p(x)$ on every interior sub-interval of $(-\infty, \infty)$.

This Lemma is a restatement of Theorem 2.1 in [45]. The implication of this Lemma is that priors for images, videos, light-fields and other visual signals can all be approximated using a GMM prior with appropriate number of mixtures, thereby allowing our framework to be applied to analyze a wide range of computational imaging systems.

- **Analytical Tractability:** Unlike other state-of-the-art signal priors such as dictionary learning [2], [35] and BM3D [12], we can analytically compute a good lower bound on MMSE [16] as described in section 4.1.

3.4 Performance Characterization

We characterize the performance of multiplexed imaging systems under (a) the noise model described in section 3.2 and (b) the scene prior model described in section 3.3. For a given multiplexing matrix H , we will study two metrics of interest: (1) $mmse(H)$, which is the minimum mean squared error (MMSE) and (2) multiplexing SNR gain $G(H)$ defined as the SNR gain (in dB) of the multiplexed system H over that of the impulse imaging system whose H -matrix is the identity matrix I :

$$G(H) = 10\log_{10}\left(\frac{mmse(I)}{mmse(H)}\right). \quad (3)$$

4 ANALYTIC PERFORMANCE CHARACTERIZATION OF CI SYSTEMS USING GMM PRIOR

We now derive an expression for the MMSE of a given camera (parameterized by the multiplexing matrix H) in terms of the noise parameters, and the learned GMM prior parameters. A GMM distribution is specified by the number of Gaussian mixtures K , the probability of each Gaussian mixture α_k , and the mean and covariance matrix (m_k, Σ_k) of each Gaussian:

$$P(x) = \sum_{k=1}^K \alpha_k \mathcal{N}(m_k, \Sigma_k). \quad (4)$$

From the given noise model, we obtain the likelihood distribution of measurements $P(y|x)$. We then compute the posterior distribution of x , $P(x|y)$, for a given y . And finally we obtain the MMSE estimator of x (which is the mean of the posterior distribution) and the corresponding MSE as a function of H .

4.1 MMSE Derivation

As discussed in section 3.2, we model the signal independent and dependent noises using Gaussian noise model. Let the noise be distributed as $\mathcal{N}(0, \Sigma_n)$. From Eqn. (1), the likelihood distribution of the measurement y is given by $P(y|x) = \mathcal{N}(Hx, \Sigma_n)$. The benefit of using a GMM prior model becomes immediately apparent after applying Bayes rule, where it can be shown that the posterior distribution $P(x|y)$ is also a GMM distribution [16] with new weights $\tilde{\alpha}_k(y)$ and new Gaussian mixture distributions $P_k(x|y)$:

$$P(x|y) = \sum_{k=1}^K \widetilde{\alpha}_k(y) P_k(x|y). \quad (5)$$

$P_k(x|y)$ is the posterior distribution of the k^{th} Gaussian

$$P_k(x|y) = \mathcal{N}(\widetilde{m}_k(y), \widetilde{\Sigma}_k) \quad (6)$$

with mean

$$\widetilde{m}_k(y) = m_k + \Sigma_k H^T (H \Sigma_k H^T + \Sigma_n)^{-1} (y - H m_k), \quad (7)$$

and covariance matrix

$$\widetilde{\Sigma}_k = \Sigma_k - \Sigma_k H^T (H \Sigma_k H^T + \Sigma_n)^{-1} H \Sigma_k. \quad (8)$$

The new weights $\widetilde{\alpha}_k(y)$ are the old weights α_k modified by the probability of y belonging to the k^{th} Gaussian mixture

$$\widetilde{\alpha}_k(y) = \frac{\alpha_k P_k(y)}{\sum_{i=1}^K \alpha_i P_i(y)}, \quad (9)$$

where $P_k(y)$, which is the probability of y belonging to the k^{th} Gaussian mixture, is given by:

$$P_k(y) = \mathcal{N}(y; H m_k, H \Sigma_k H^T + \Sigma_n) \quad (10)$$

The MMSE estimator $\hat{x}(y)$ is the mean of the posterior distribution $P(x|y)$, i.e.,

$$\hat{x}(y) = \sum_{k=1}^K \widetilde{\alpha}_k(y) \widetilde{m}_k(y), \quad (11)$$

and the MMSE is given by

$$\begin{aligned} mmse(H) &= E \|x - \hat{x}(y)\|^2 \\ &= \int_{\mathbf{y}} \left(\int_{\mathbf{x}} \|x - \hat{x}(y)\|^2 P(x|y) dx \right) P(y) dy, \end{aligned} \quad (12)$$

where $P(y)$ is the marginal distribution of y and is given by [16]:

$$P(y) = \sum_{i=1}^K \alpha_i P_i(y), \quad (13)$$

with $P_k(y)$ defined as in Eqn. (10).

The $mmse(H)$ can be written as a sum of two terms: an *intra-mixture* error term and an *inter-mixture* error term.

$$\begin{aligned} mmse(H) &= \sum_{k=1}^K \alpha_k Tr(\widetilde{\Sigma}_k) \\ &+ \sum_{k=1}^K \alpha_k \int_{\mathbf{y}} \|\hat{x}(y) - \widetilde{m}_k(y)\|^2 P_k(y) dy, \end{aligned} \quad (14)$$

where Tr denotes matrix trace. The first term is the *intra-mixture* error, which is given by the mean MSE for the case when y (which is sampled from one of the K Gaussian mixtures) is classified to the correct Gaussian mixture. The

second term is the *inter-mixture* error, which is the MSE due to inter-mixture confusion. The proof for the above decomposition is given in Appendix A. After a quick look back to Eqn. (8), it can be seen that the first term in Eqn. (14) is independent of the observation y and depends only on the multiplexing matrix H , the noise covariance Σ_n , and the learned GMM prior parameters α_k , m_k , and Σ_k .

Performance Bound for CI with Signal Priors. Unfortunately we need Monte-Carlo simulations to compute the second term in Eqn. (14). However, we can use the first term as a lower bound on MMSE (and hence upper bound on SNR), i.e.,

$$mmse(H) \geq \sum_{k=1}^K \alpha_k Tr(\widetilde{\Sigma}_k), \quad (15)$$

Eqn. (15) bounds the performance of any camera, and can be computed analytically from only the parameters for the camera, noise, and learned signal prior. For fully-determined systems at low noise condition (high lighting level) we can expect this lower bound to be tight. In fact we have observed the same in our experiments. Thus, in the future, this lower bound alone could be used to optimize CI systems in the presence of signal priors.

4.2 Incorporating the Noise Model

For signal independent noise, we assume noise to be isotropic with variance σ_r^2 . As discussed in section 3.2, we approximate the signal dependent noise n by signal independent Gaussian noise with variance equal to the average value of the captured signal. Note that the increase in light gathering power, and hence also signal-dependent noise, is implicitly encoded in the multiplexing matrix H . The total light gathering power for a given pixel is determined by the row-sum of H . Let $C(H)$ be the matrix light throughput, defined as the average row sum of H , and let m be the pixel mean of the impulse image, then the photon noise variance is $\sigma_p^2 = m \cdot C(H)$, and the total noise is modeled as

$$P(n|x) = \mathcal{N}(0, \Sigma_n), \quad \Sigma_n = (\sigma_r^2 + \sigma_p^2) \mathcal{I}$$

The corresponding MMSE estimator, MMSE and the lower bound on MMSE are given by Eqn. (11), (14) and (15) respectively with $\Sigma_n = (\sigma_r^2 + \sigma_p^2) \mathcal{I}$.

5 COMMON FRAMEWORK FOR ANALYSIS OF CI SYSTEMS

We study the performance of various CI systems under the practical consideration of illumination conditions and sensor characteristics.

5.1 Performance Characterization

Computational Imaging (CI) systems improve upon traditional imaging systems by allowing more light to be captured by the sensor. However, captured images then require decoding, which typically results in noise amplification. To improve upon performance, the benefit of increased light

Relation between light levels and average photon counts for different camera types









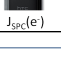
	 Quarter moon	 Full moon	 Twilight	 Indoor lighting	 Cloudy day	 Sunny day
I_{src} (lux)	10^{-2}	1	10	10^2	10^3	10^4
 $J_{SLR}(e^-)$	8×10^{-3}	0.8	8.1	81.4	814.3	8143
 $J_{MVC}(e^-)$	7.9×10^{-4}	7.9×10^{-2}	0.79	7.9	79.5	7952
 $J_{SPC}(e^-)$	1.3×10^{-4}	1.3×10^{-2}	0.13	1.27	12.7	127

Fig. 2. *Relation between light levels and average signal levels for different camera specifications:* Given the illumination level and camera specifications, the average signal level J of the impulse imaging system is computed using Eqn. (16). We consider three typical camera specifications: 1) a high end SLR camera, 2) a machine vision camera (MVC) and 3) a smartphone camera (SPC). See section 5.3 for the chosen camera parameter values.

throughput needs to outweigh the degradations caused by the decoding process. The combined effect of these two processes is measured as the SNR gain.

To calculate the SNR gain, we need to first define an appropriate baseline. Following the approach of [10], we choose impulse imaging as the baseline for comparison. This corresponds to a traditional camera with a stopped down aperture (so that entire scene is within depth of field) or a short exposure duration (so as to avoid motion blur) for EDOF and motion deblurring systems, respectively.

The baseline chosen by [10] does not address the fact that impulse imaging performance can be significantly improved upon by state of the art image denoising methods [12], [6], [31]. We correct this by denoising our impulse images using the GMM prior. The effect this has on performance is clearly seen in Figure 1. The dotted blue line corresponds to impulse imaging without denoising, while the solid blue line corresponds to impulse imaging after denoising using the GMM prior. Thus, the results presented in Figures 4, 5 show the performance improvements obtained due to CI above and beyond the performance of impulse imaging with state of the art denoising. Another important result of this paper, is that much like [6], [31], we are also able to quantify the significant performance improvements that can be obtained through image denoising.

5.2 Scene Illumination Level

The primary variable that controls the SNR of impulse imaging is the scene illumination level. As discussed in section 3.2, we consider two noise types: photon noise (signal dependent) and read noise (signal independent). Photon noise is directly proportional to the scene illumination level, whereas, read noise is independent of it. At low illumination levels, read noise dominates the photon noise but, since signal power is low, the SNR is typically low. At

high scene illumination levels, photon noise dominates the read noise. Recognizing this, we compare CI techniques to impulse imaging over a wide range of scene illumination levels, as shown in Figure 2. Our results show that over the entire range of scene illuminations, CI techniques provide performance benefits, as seen in Figures 4 and 5.

5.3 Imaging System Specification

The actual relationship between scene illumination (in lux) and the signal level captured by sensor depends upon camera characteristics such as the f-number (ratio of focal length to the aperture size) and exposure time, and sensor parameters such as quantum efficiency and pixel size. Here, we choose three different example cameras that span the a wide range of consumer imaging devices: 1) a high end SLR camera, 2) a machine vision camera (MVC) and 3) a smartphone camera (SPC). For each of these example camera types, we choose parameters that are typical in the marketplace today: sensor pixel size: $\delta_{SLR} = 8\mu m$ for the SLR camera, $\delta_{MVC} = 2.5\mu m$ for the MVC, and $\delta_{SPC} = 1\mu m$ for the SPC. We also assume a sensor read noise of $\sigma_r = 4e^-$ which is typical for today's CMOS sensors.

Given the scene illumination level I_{src} (in lux), the average scene reflectivity (R) and the camera parameters such as the f-number ($F/\#$), exposure time (t), sensor quantum efficiency (q), and pixel size (δ), the average signal level in photo-electrons (J) of the impulse camera is given by [10]¹:

$$J = 10^{15} (F/\#)^{-2} t I_{src} R q (\delta)^2. \quad (16)$$

In our experiments, we assume an average scene reflectivity of $R = 0.5$ and sensor quantum efficiency of $q = 0.5$, aperture setting of $F/11$ and exposure time of $t = 6$ milliseconds, which are typical settings in consumer photography. Figure 2 shows the average signal values J for the three camera settings and some typical scene illumination levels.

Sensor characteristics impact the SNR directly: sensors with larger pixels produce a higher SNR at the same scene illumination level. The x-axis of the plots shown in Figures 1, 4 and 5 for SLR, MVC and the SPC are simply shifted relative to one another. Note that CI techniques provide quantifiable performance improvements over the entire range of lighting and sensor characteristics.

5.4 Experimental Details

The details of the experimental setup are as follows

- **Learning:** We learn GMM patch priors from a large collection of about 50 million training patches. For learning we use a variant of the Expectation Maximization approach to ascertain the model parameters. We also test that the learned model is an adequate approximation of the real image prior by performing

1. The signal level will be larger for CI techniques. The increase in signal is encoded in the multiplexing matrix H , as discussed in Section 4

rigorous statistical analysis and comparing performance of the learned prior with state of the art image denoising methods [12].

- **Analytic Performance metric:** Analytic performance is compared using the MMSE metric. Once the MMSE is computed for the impulse and CI systems, we compute the multiplexing SNR gain in dB using Eqn. (3). The analytic multiplexing gain for various CI systems are shown in Figures 1, 4 and 5(a).
- **Analytic Performance without Prior:** To calculate the performance of CI systems without signal priors taken into account, we compute the MSE as:

$$mse(H) = Tr(H^{-1}\Sigma_n H^{-T}), \quad (17)$$

where H is the corresponding multiplexing matrix and Σ_n is the noise covariance matrix.

- **Analytic Performance with Prior:** The analytic performance of CI systems with priors taken into account is computed as described in Section 4 (Eqn. (14)). These results are shown in Figures 1, 4 and 5(a).
- **Simulations Results for Comparison:** In order to validate our analytic predictions, we also performed extensive simulations. In our simulations, we used the MMSE estimator, Eqn. (11), to reconstruct the original (sharp) images. The MMSE estimator has been shown to provide state of art results for image denoising [31], and here we extend these powerful methods for general demultiplexing. Some images of our simulation experiments are shown in Figures 3 and 5(b), providing visual and qualitative comparison between CI and traditional imaging techniques. The simulation results are consistent with our analytic predictions and show that CI provides performance benefits over a wide range of imaging scenarios.

6 PERFORMANCE ANALYSIS OF EDOF SYSTEMS

We study the SNR gain of various EDOF systems with and without the use of signal priors. For the signal prior, we learn a GMM patch prior, of patch size 16×16 , with 1770 Gaussian mixtures. First we study the performance of a particular EDOF system, focal sweep [26], and compare it with impulse imaging. We assume the aperture size of the focal sweep system to be 11×11 times bigger than that of the impulse camera, corresponding to an aperture setting of $F/1$. Hence, the light throughput of focal sweep is about 121 times that of the impulse camera. Figure 1 shows the analytical SNR gain for focal sweep and impulse cameras with and without using signal prior. The plot shows performance measured relative to impulse imaging without a signal prior (no denoising). Without the prior, focal sweep has a huge SNR gain over impulse imaging at low photon to read noise ratio, J/σ_r^2 . This is consistent with the result obtained in [10]. However, when the signal prior is taken into account, the SNR gain is modest even at low J/σ_r^2 . From the plot it is also clear that the the use of prior

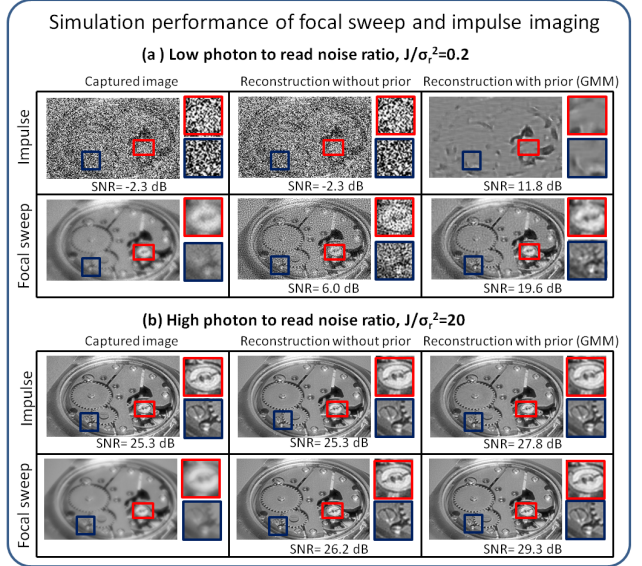


Fig. 3. *Simulation performance of focal sweep [26] and impulse cameras:* Subplots (a) and (b) show the simulation results obtained by focal sweep and impulse imaging for low ($J/\sigma_r^2 = 0.2$) and high ($J/\sigma_r^2 = 20$) photon to read noise ratios. For the low photon to read noise ratio case, the use of prior increases SNR by around 14dB for both focal sweep and impulse imaging. Multiplexing increases SNR by about 8 dB regardless of the use of prior. For the high photon to read noise ratio case, the SNR gains due to both prior and multiplexing decrease.

increases SNR more than does multiplexing. Figure 3(a-b) shows the simulation results obtained from focal sweep and impulse imaging for a low ($J/\sigma_r^2 = 0.2$) and a high ($J/\sigma_r^2 = 20$) photon to read noise ratios. In the low photon to read noise ratio case, the use of prior increases SNR by around 14dB for both focal sweep and impulse imaging. Multiplexing increases SNR by about 8 dB regardless of the use of prior. When the ratio of photon to read noise is large, the SNR gains due to both prior and multiplexing decrease.

Further, we study the performance of various other EDOF systems such as cubic phase wavefront coding [13], and the coded aperture designs by Zhou et al. [53] and Levin et al. [28]². Figure 4 shows the SNR gain (in dB) of these EDOF systems with respect to impulse imaging *with a signal prior* (denoising). Wavefront coding achieves a peak SNR gain of 8.8 dB and an average SNR gain of about 7 dB.

Practical Implications: The main conclusions of our analysis are

- *The use of signal priors improves the performance of both CI and impulse imaging significantly.*
- *Good EDOF systems are about 7 dB better than*

2. The performance of coded aperture systems reported here is overoptimistic because we assume perfect kernel estimation, as discussed in Section 1.

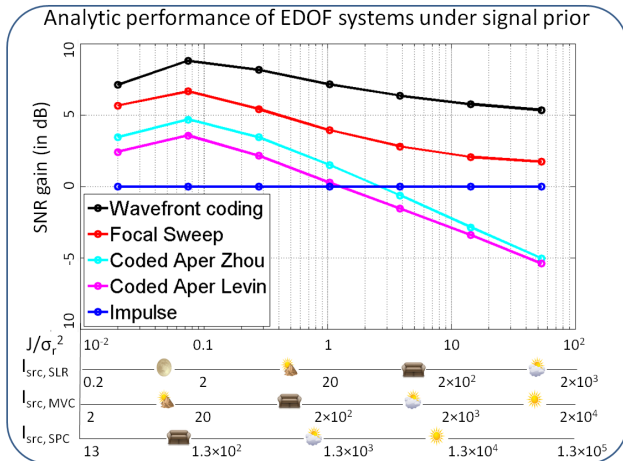


Fig. 4. Comparison of EDOF systems when signal priors are taken into account: We plot the SNR gain of various EDOF systems at different photon to read noise ratios (J/σ_r^2). In the extended x-axis, we also show the effective illumination levels (in lux) required to produce the given J/σ_r^2 for the three camera specifications: SLR, MVC and SPC. The EDOF systems that we consider are: cubic phase wavefront coding [13], focal sweep camera [26], and the coded aperture designs by Zhou et al. [53] and Levin et al. [28]. Signal priors are used to improve performance for both CI and impulse cameras. Wavefront coding achieves a peak SNR gain of 8.8 dB and an average SNR gain of about 7 dB.

comparable impulse imaging systems after the effect of signal priors are taken into account, thus demonstrating the benefits of multiplexing above and beyond those of non-linear reconstruction algorithms.

- Contrary to previous results [10], our analysis shows that CI systems confer significant performance benefits over impulse imaging over a wide range of illumination levels and camera specifications.

7 PERFORMANCE ANALYSIS OF MOTION DEBLURRING SYSTEMS

We study the performance of two motion deblurring systems: the flutter shutter [41] and motion invariant camera [33]. Again, we focus our attention on the case where signal priors are taken into account. For this experiment, we learn a GMM patch prior, of patch size 4×256 , with 1900 Gaussian mixtures. For the motion deblurring cameras, we set the exposure time to be 33 times that of the impulse camera, corresponding to an exposure time of 200 milliseconds. The binary flutter shutter code that we used in our experiment has 15 'ones' and hence the light throughput is 15 times that of the impulse imaging system. The light throughput of the motion invariant camera is 33 times that of the impulse camera. Figure 5(a) shows the analytic SNR gain (in dB) of the motion deblurring systems with respect to impulse imaging *when signal priors are taken into account*³. Motion invariant imaging achieves

3. Flutter shutter performance reported here is overoptimistic because we assume perfect kernel estimation, as discussed in Section 1.

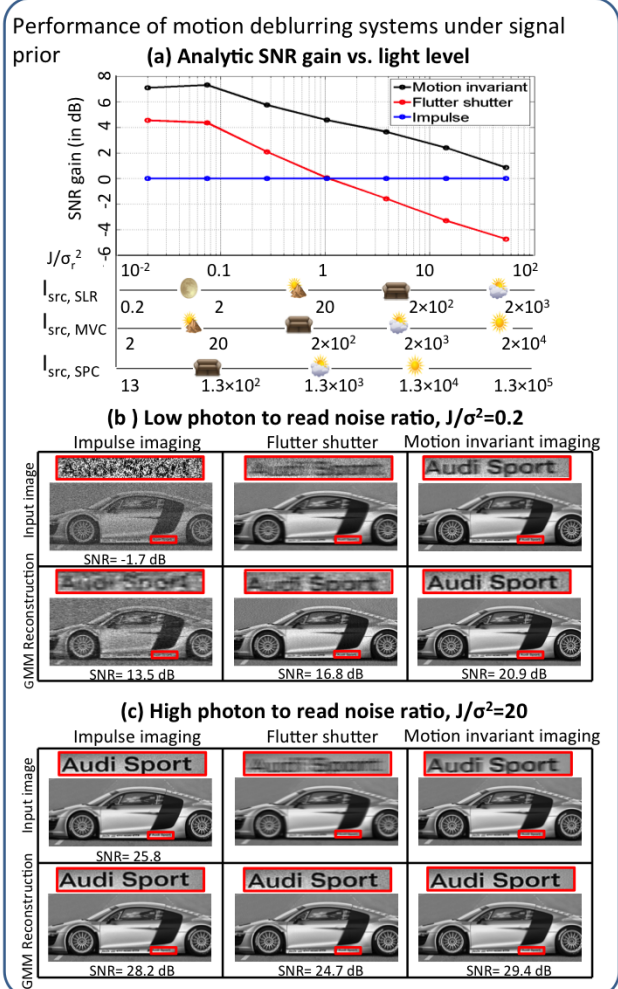


Fig. 5. Comparison of motion deblurring cameras: We study the performance of motion invariant [33], flutter shutter [41] and impulse cameras when image priors are taken into account. Subplot (a) shows the analytic SNR gain (in dB) vs. photon to read noise ratio J/σ_r^2 for the two motion deblurring systems. In the extended x-axis, we also plot the corresponding light levels (in lux) for the three different camera specifications: SLR, MVC and SPC. The motion invariant camera achieves a peak SNR gain of 7.3 dB and an average SNR gain of about 4.5 dB. Subplots (b-c) show the corresponding simulation results. At a low photon to read noise ratio of $J/\sigma_r^2 = 0.2$, motion invariant imaging performs 7.4 dB better than impulse imaging. At the high photon to read noise ratio of $J/\sigma_r^2 = 20$, it is only 1.2 dB better.

a peak SNR gain of 7.3 dB and an average SNR gain of about 4.5 dB. Figure 5(b-c) show the corresponding simulation results. At the low photon to read noise ratio of $J/\sigma_r^2 = 0.2$, motion invariant imaging performs 7.4 dB better than impulse imaging. At the high photon to read noise ratio of $J/\sigma_r^2 = 20$, it is only 1.2 dB better. Also, the use of prior alone increases the performance of impulse imaging by 15.2 dB for the low photon to read noise case and by 2.4 dB for the high photon to read noise case. CI systems also show similar increases due to the use of prior alone.

Practical Implications: The main conclusion of our analysis is

- *The use of signal priors improves the performance of both CI and impulse imaging significantly.*
- *Good multiplexed motion deblurring systems perform 4.5 dB better than impulse imaging after signal priors are taken into account. Performance is consistently better than impulse imaging for a wide range of illumination conditions and camera specifications.*

8 DISCUSSIONS

We present a framework to comprehensively analyze the performance of CI systems. Our framework takes into account the effect of multiplexing, affine noise and signal priors. We model signal priors using a GMM, which can approximate almost all prior signal distributions. More importantly, the prior is analytically tractable. We use the MMSE metric to characterize the performance of any given linear CI system. Our analysis allows us to determine the increase in performance of CI systems *when signal priors are taken into account*. We use our framework to analyze several CI techniques, including both EDOF and motion deblurring cameras. Our analysis reveals that: 1) Multiplexing gain is much more modest when signal priors are taken into account, and 2) Signal priors increase SNR more than multiplexing. Moreover, we use our framework to establish the following practical implications: 1) Good EDOF systems can achieve a multiplexing gain of 7 dB over impulse imaging, and 2) Good motion deblurring system can perform 4.5 dB better than impulse imaging.

While the results reported in this paper are specific to EDOF and motion deblurring cameras, the framework can be applied to analyze any linear CI camera. In the future, we would like to use our framework to learn priors and analyze multiplexing performance for other types of datasets (e.g. videos, hyperspectral volumes, light fields, reflectance fields). Of particular interest is the analysis of compressive CI techniques. Analyzing the performance of compressed sensing matrices has been a notoriously difficult problem, except in a few special cases (e.g. Gaussian, Bernouli, and Fourier matrices). Our framework can gracefully handle any arbitrary multiplexing matrix, and thus could prove to be a significant contribution to the compressed sensing community. By the same token, we would like to apply our analysis to overdetermined systems so that we may also analyze multiple image capture CI techniques (e.g. Hasinoff et al. [22] and Zhang et al. [52]). Finally, and perhaps most significantly, we would like to apply our framework towards the problem of parameter optimization for different CI techniques. For instance, we may use our framework to determine the optimal aperture size for focal sweep cameras, the optimal flutter shutter code for motion deblurring, or the optimal measurement matrix for a compressed sensing system. In this way, we believe our framework can be used to exhaustively analyze the field of CI research and provide invaluable answers to existing open questions in the field.

9 APPENDIX A: DERIVATION OF MMSE FOR GMM PRIOR

We show that the MMSE can be written as the sum of two terms: an intra-mixture error term and an inter-mixture error term, see Eqn. (14). The original expression of MMSE is given by Eqn. (12). Let us first concentrate on the inner integral in Eqn. (12):

$$\int_x ||x - \hat{x}(y)||^2 P(x|y) dx. \quad (18)$$

Using the expression for $P(x|y)$ in Eqn. (5), the above integral can be written as

$$\sum_{k=1}^K \tilde{\alpha}_k(y) \int_x ||x - \hat{x}(y)||^2 P_k(x|y) dx.$$

We then add and subtract $\tilde{m}_k(y)$ to obtain

$$\sum_{k=1}^K \tilde{\alpha}_k(y) \int_x ||x - \tilde{m}_k(y) + \tilde{m}_k(y) - \hat{x}(y)||^2 P_k(x|y) dx.$$

Using the expansion $||a+b||^2 = ||a||^2 + ||b||^2 + 2a^T b$ with $a = x - \tilde{m}_k(y)$ and $b = \tilde{m}_k(y) - \hat{x}(y)$ and keeping in mind that the term b is independent of x , we get

$$\begin{aligned} & \sum_{k=1}^K \tilde{\alpha}_k(y) \int_x ||x - \tilde{m}_k(y)||^2 P_k(x|y) dx \\ & + \sum_{k=1}^K \tilde{\alpha}_k(y) ||\tilde{m}_k(y) - \hat{x}(y)||^2 \\ & + \sum_{k=1}^K \tilde{\alpha}_k(y) (\tilde{m}_k(y) - \hat{x}(y))^T \int_x (x - \tilde{m}_k(y)) P_k(x|y) dx. \end{aligned}$$

Since, $P_k(x|y)$ is a Gaussian distribution with mean $\tilde{m}_k(y)$ and covariance $\tilde{\Sigma}_k$, see Eqn. (6), we can rewrite the above expression as

$$\sum_{k=1}^K \tilde{\alpha}_k(y) Tr(\tilde{\Sigma}_k) + \sum_{k=1}^K \tilde{\alpha}_k(y) ||\tilde{m}_k(y) - \hat{x}(y)||^2.$$

Thus, till now, we have shown that the inner integral of the MMSE, Eqn. (18), is given by the above expression. Now we consider the outer integral in Eqn. (12).

Taking the outer integral into account, the MMSE can be written as

$$\begin{aligned} & \sum_{k=1}^K Tr(\tilde{\Sigma}_k) \int_y \tilde{\alpha}_k(y) P(y) dy \\ & + \sum_{k=1}^K \int_y ||\tilde{m}_k(y) - \hat{x}(y)||^2 \tilde{\alpha}_k(y) P(y) dy. \end{aligned}$$

Using the definitions of $\tilde{\alpha}_k(y)$, Eqn. (9), and $P(y)$, Eqn. (13), we can rewrite the above expression as

$$\sum_{k=1}^K \alpha_k \text{Tr}(\widetilde{\Sigma}_k) + \sum_{k=1}^K \alpha_k \int_y \|\widetilde{m}_k(y) - \hat{x}(y)\|^2 P_k(y) dy,$$

which expresses the MMSE as the sum of the intra-mixture and inter-mixture terms, as in Eqn. (14).

REFERENCES

- [1] A. Agarwal and R. Raskar. Optimal single image capture for motion deblurring. In *CVPR*, 2009. 3
- [2] M. Aharon, M. Elad, and A. Bruckstein. k-svd: An algorithm for designing overcomplete dictionaries for sparse representation. *IEEE Transactions on Signal Processing*, 54(11):4311–4322, 2006. 2, 4
- [3] J. Baek. Transfer Efficiency and Depth Invariance in Computational Cameras. In *ICCP*, 2010. 3
- [4] R. Baer, W. Holland, J. Holm, and P. Vora. A comparison of primary and complementary color filters for ccd-based digital photography. In *SPIE Electronic Imaging Conference*. Citeseer, 1999. 1
- [5] A. Castro and J. Ojeda-Castañeda. Asymmetric phase masks for extended depth of field. *Appl. Opt.*, 43(17):3474–3479, Jun 2004. 1
- [6] P. Chatterjee and P. Milanfar. Is denoising dead? *Image Processing, IEEE Transactions on*, 19(4):895–911, 2010. 3, 6
- [7] M. Chen, J. Silva, J. Paisley, C. Wang, D. Dunson, and L. Carin. Compressive sensing on manifolds using a nonparametric mixture of factor analyzers: Algorithm and performance bounds. *IEEE Transactions on Signal Processing*, 58(12):61406155, December 2010. 4
- [8] T. Cho, A. Levin, F. Durand, and W. Freeman. Motion blur removal with orthogonal parabolic exposures. In *ICCP*, 2010. 1, 2, 3
- [9] O. Cossairt. Tradeoffs and Limits in Computational Imaging (Ph.D. Thesis). Technical report, Sep 2011. 1, 2, 3
- [10] O. Cossairt, M. Gupta, and S. K. Nayar. When does computational imaging improve performance? *IEEE transactions on image processing*, 22(1-2):447–458, 2013. 1, 2, 3, 6, 7, 8
- [11] O. Cossairt, C. Zhou, and S. K. Nayar. Diffusion Coding Photography for Extended Depth of Field. In *SIGGRAPH*, 2010. 3
- [12] K. Dabov, A. Foi, V. Katkovnik, and K. Egiazarian. Image denoising by sparse 3-d transform-domain collaborative filtering. *TIP*, 16(8), 2007. 2, 4, 6, 7
- [13] E. Dowski Jr and W. Cathey. Extended depth of field through wavefront coding. *Applied Optics*, 34(11):1859–1866, 1995. 1, 2, 7, 8
- [14] Y. C. Eldar, P. Kuppinger, and H. Bolcskei. Block-sparse signals: Uncertainty relations and efficient recovery. *IEEE Transactions on Signal Processing*, 58(6):30423054, November 2010. 4
- [15] Y. C. Eldar and M. Mishali. Robust recovery of signals from a structured union of subspaces. *IEEE Transactions on Information Theory*, 55(11):53025316, November 2009. 4
- [16] J. T. Flam, S. Chatterjee, K. Kansanen, and T. Ekman. Minimum mean square error estimation under gaussian mixture statistics. *arXiv:1108.3410*, 2011. 4, 5
- [17] E. E. García-Guerrero, E. R. Méndez, H. M. Escamilla, T. A. Leskova, and A. A. Maradudin. Design and fabrication of random phase diffusers for extending the depth of focus. *Opt. Express*, 15(3):910–923, Feb 2007. 1
- [18] N. George and W. Chi. Extended depth of field using a logarithmic asphere. *Journal of Optics A: Pure and Applied Optics*, 2003. 1
- [19] J. A. Guerrero-Colon, L. Mancera, and P. J. Image restoration using space-variant gaussian scale mixtures in overcomplete pyramids. *IEEE Transactions on Image Processing*, 17(1):2741, January 2008. 4
- [20] Q. Hanley, P. Verveer, and T. Jovin. Spectral imaging in a programmable array microscope by hadamard transform fluorescence spectroscopy. *Applied Spectroscopy*, 53(1), 1999. 1
- [21] M. Harwit and N. Sloane. Hadamard transform optics. *New York: Academic Press*, 1979. 1, 2, 3
- [22] S. Hasinoff, K. Kutulakos, F. Durand, and W. Freeman. Time-constrained photography. In *ICCV*, pages 1–8, 2009. 2, 3, 4, 9
- [23] S. W. Hasinoff, K. N. K. F. Durand, and W. T. Freeman. Light-efficient photography. In *ECCV*, 2008. 1, 2
- [24] G. Häusler. A method to increase the depth of focus by two step image processing. *Optics Communications*, 1972. 1, 2
- [25] I. Ihrke, G. Wetzstein, and W. Heidrich. A theory of plenoptic multiplexing. In *CVPR*, 2010. 1, 2, 3, 4
- [26] S. Kuthirummal, H. Nagahara, C. Zhou, and S. K. Nayar. Flexible Depth of Field Photography. In *PAMI*, 2010. 1, 2, 7, 8
- [27] D. Lanman, R. Raskar, A. Agrawal, and G. Taubin. Shield fields: modeling and capturing 3d occluders. In *SIGGRAPH*, 2008. 1
- [28] A. Levin, R. Fergus, F. Durand, and W. Freeman. Image and depth from a conventional camera with a coded aperture. In *SIGGRAPH*. ACM, 2007. 1, 2, 3, 4, 7, 8
- [29] A. Levin, W. T. Freeman, and F. Durand. Understanding camera trade-offs through a bayesian analysis of light field projections. In *ECCV*, pages 88–101, 2008. 3
- [30] A. Levin, S. W. Hasinoff, P. Green, F. Durand, and W. T. Freeman. 4d frequency analysis of computational cameras for depth of field extension. *ACM Trans. Graph.*, 28(3), 2009. 1
- [31] A. Levin and B. Nadler. Natural image denoising: Optimality and inherent bounds. In *Computer Vision and Pattern Recognition (CVPR), 2011 IEEE Conference on*, pages 2833–2840. IEEE, 2011. 3, 6, 7
- [32] A. Levin, B. Nadler, F. Durand, and W. T. Freeman. Patch complexity, finite pixel correlations and optimal denoising. In *ECCV (5)*, pages 73–86, 2012. 3
- [33] A. Levin, P. Sand, T. Cho, F. Durand, and W. Freeman. Motion-invariant photography. In *SIGGRAPH*, 2008. 1, 2, 3, 8
- [34] C. Liang, T. Lin, B. Wong, C. Liu, and H. Chen. Programmable aperture photography: multiplexed light field acquisition. In *SIGGRAPH*, 2008. 1
- [35] J. Mairal, F. Bach, J. Ponce, and G. Sapiro. Online learning for matrix factorization and sparse coding. *Journal of Machine Learning Research*, 11:19–60, 2010. 4
- [36] K. Mitra and A. Veeraraghavan. Light field denoising, light field superresolution and stereo camera based refocusing using a gmm light field patch prior. In *CVPR Workshops*, 2012. 2, 4
- [37] S. Nayar. Computational camera: Approaches, benefits and limits. Technical report, DTIC Document, 2011. 1
- [38] R. Ng, M. Levoy, M. Brédif, G. Duval, M. Horowitz, and P. Hanrahan. Light field photography with a hand-held plenoptic camera. *Computer Science Technical Report*, 2, 2005. 1
- [39] J. Ojeda-Castaneda, J. E. A. Landgrave, and H. M. Escamilla. Annular phase-only mask for high focal depth. *Optics Letters*, 2005. 1
- [40] K. N. Plataniotis and D. Hatzinakos. gaussian mixtures and their applications to signal processing. pages 3.2 – 3.32, December 2000. 2, 4
- [41] R. Raskar, A. Agrawal, and J. Tumblin. Coded exposure photography: motion deblurring using fluttered shutter. In *SIGGRAPH*, 2006. 1, 2, 3, 8
- [42] N. Ratner and Y. Schechner. Illumination multiplexing within fundamental limits. In *CVPR*, 2007. 1, 2, 3
- [43] N. Ratner, Y. Schechner, and F. Goldberg. Optimal multiplexed sensing: bounds, conditions and a graph theory link. *Optics Express*, 15, 2007. 3
- [44] Y. Schechner, S. Nayar, and P. Belhumeur. Multiplexing for optimal lighting. *Pattern Analysis and Machine Intelligence, IEEE Transactions on*, 29(8):1339–1354, 2007. 1, 2, 4
- [45] H. W. Sorenson and D. L. Alspach. Recursive bayesian estimation using gaussian sums. *Automatica*, 7:465–479, 1971. 2, 4
- [46] Y. Tendo. Mathematical theory of the flutter shutter. *PhD. Thesis, ENS Cachan*, 2012. 3
- [47] A. Veeraraghavan, R. Raskar, A. Agrawal, A. Mohan, and J. Tumblin. Dappled photography: Mask enhanced cameras for heterodyned light fields and coded aperture refocusing. *SIGGRAPH*, 2007. 1, 2, 3, 4
- [48] A. Wagadarikar, R. John, R. Willett, and D. Brady. Single disperser design for coded aperture snapshot spectral imaging. *Applied optics*, 47(10):B44–B51, 2008. 1, 3, 4
- [49] A. Wuttig. Optimal transformations for optical multiplex measurements in the presence of photon noise. *Applied Optics*, 44, 2005. 2, 3
- [50] J. Yang, X. Yuan, X. Liao, P. Llull, D. J. Brady, G. Sapiro, and L. Carin. Video compressive sensing using gaussian mixture models. 2013. 4
- [51] G. Yu, G. Sapiro, and S. Mallat. Solving inverse problems with piecewise linear estimators: From gaussian mixture models to structured sparsity. *IEEE Transactions on Image Processing*, (5), 2012. 2, 4
- [52] L. Zhang, A. Deshpande, and X. Chen. Denoising versus Deblurring: HDR techniques using moving cameras. In *CVPR*, 2010. 3, 9
- [53] C. Zhou and S. Nayar. What are Good Apertures for Defocus Deblurring? In *ICCP*, 2009. 1, 2, 3, 7, 8